

Interband pairing theory of superconductivity

Jamil Tahir-Kheli

First Principles Research, Inc., 8391 Beverly Boulevard, Suite No. 171, Los Angeles, California 90048

(Received 8 September 1997)

A model for high-temperature superconductors based on the idea of Cooper pairs comprised of electrons from *different* bands is studied. We propose that the two bands relevant for the cuprates are comprised of Cu $d_{x^2-y^2}$, d_{z^2} , planar O p_σ , and apical O p_z orbitals. Along the diagonal, $k_x=k_y$ in the Brillouin zone, the two-band Fermi surfaces may cross. We associate the optimal doping for the highest T_c with this point because only in the vicinity of this touching point are interband Cooper pairs energetically possible. Due to the lack of time-reversal invariance of an interband Cooper pair with itself, the standard interpretation of Josephson tunneling is altered such that the detailed nature of the single-particle tunneling matrix elements contributes to the supercurrent. The $d_{x^2-y^2}$ gap observations from Josephson tunneling are shown to arise from our model with pairing due to phonons. A Hubbard model is written down for the two bands at the Fermi energy with realistic parameters for $\text{La}_{1.85}\text{Sr}_{0.15}\text{CuO}_4$. The anomalous normal-state features in the NMR are calculated and qualitatively explained as due to the character of the two bands in the vicinity of the crossing point. The Hall effect is calculated using standard Bloch-Boltzmann transport theory. The observed strong temperature dependence of the Hall coefficient is reproduced and is due to the strong reshaping of the current-carrying band Fermi surface due to band repulsion with the other band for dopings very close to the Fermi-surface touching point. Reasonable quantitative agreement is also obtained for the NMR and Hall effect. A linear resistivity at optimal doping is expected due to the proximity of the second band in k space which can strongly relax the current and the “smallness” of the current-carrying Fermi surface. [S0163-1829(98)04142-3]

I. INTRODUCTION

In a previous publication the author proposed an interband pairing (IBP) model for high-temperature superconductors.¹ We suggested that the fundamental idea of Cooper pairs composed of electrons in states $k\uparrow$ and $-k\downarrow$ be retained but rather than $k\uparrow$ and $-k\downarrow$ being from the same band, we consider pairs such that $k\uparrow$ and $-k\downarrow$ come from *different* bands at the Fermi surface. Such Cooper pairs, if they exist, are not time-reversal invariant with themselves in contrast to all BCS-like (intra-band) Cooper pairs. The full Hamiltonian is time-reversal invariant, though. We showed that with such interband pairs, the orbital character of the two bands plays a significant role in all Josephson tunneling experiments. The phase difference across a junction is no longer simply the phase difference of the two gap functions but also includes a contribution due to the phases of the hopping matrix elements across the junction. With BCS-like Cooper pairs, the product of the single-particle tunneling matrix elements is mod-squared due to the time-reversal invariance of the pair. This is not the case with IBP. We suggest that the observed^{2,3} $d_{x^2-y^2}$ character of the Josephson tunneling can be resolved by an “ s -like gap” coupled with a “ $d_{x^2-y^2}$ ” Cooper pair. These issues will be explained in detail below.

Clearly, in order to have any possibility of creating an interband Cooper pair, $(k\uparrow_U, -k\downarrow_L)$ where U, L are labels for the two distinct bands (eventually taken to represent the upper and lower bands), the single-particle energies $\epsilon_k^{(U)} = \epsilon_{-k}^{(U)}$, $\epsilon_k^{(L)} = \epsilon_{-k}^{(L)}$ must be close to the Fermi energy. Such a circumstance is easily available when the U and L band Fermi surfaces intersect. Of course, bands repel each other in general unless there is a symmetry that forbids mixing. Thus,

Cooper pairing will occur in the vicinity of special symmetry points in the Brillouin zone.

Our previous paper dealt with the unphysical situation of two distinct bands with exactly coincident Fermi surfaces at a given doping which was associated with the optimal doping for superconductivity. In this regard, the previous study of IBP must be regarded as an overly simplistic model that serves to illustrate some of the general principles of IBP but cannot account for quantitative features. This paper considers realistic bands for the cuprates and derives some quantitative consequences of the theory.

We propose the two relevant bands for high- T_c are comprised predominantly of Cu $d_{x^2-y^2}$, Cu d_{z^2} , planar O p_σ , and apical O p_z orbitals. The two bands are strong mixtures of these orbitals except at special k points only. A simple Hubbard model is written down for the system. The parameters used in our Hubbard model are derived in the following paper by Perry and Tahir-Kheli⁴ using *ab initio* calculations on finite clusters for $\text{La}_{1.85}\text{Sr}_{0.15}\text{CuO}_4$. Contrary to the results of local-density approximation (LDA) band-structure calculations on the cuprates, we find two bands at the Fermi energy comprised primarily of the above orbitals. The difference between our results and previous band-structure calculations is due to correcting the self-interaction energy in LDA. The optimal doping is the doping where the two-band Fermi surfaces touch. This can happen along the diagonal where $k_x=k_y$. $\text{La}_{1.85}\text{Sr}_{0.15}\text{CuO}_4$ is primarily considered here so the three-dimensional (3D) dispersion is small.

The NMR spin-relaxation rates at the planar Cu and O nuclei are estimated with these bands and so are the respective Knight shifts. Reasonable quantitative agreement with many of the anomalous NMR properties⁵⁻¹¹ is obtained. The dramatically different temperature dependences of the planar

Cu and O spin-relaxation rates is due to the conspiring of several important aspects of the orbital characters of the two bands U and L at the Fermi energy. The major reason is that there are two possible orbitals on the Cu, $d_{x^2-y^2}$ and d_{z^2} , whereas there is only one important orbital p_σ on the planar O. The second most important reason is that the L band is almost full at optimal doping and the orbital character of the available L k states is dominated by the character at the top of the band at $k=(\pi, \pi)$.

The large spin-relaxation anisotropy¹⁰ on the Cu site is discussed and we argue this is due to a small mixture of d_{xy} character in the two bands. We show that mixing of d_{xy} of a few percent is sufficient to produce the observed anisotropy ratio of ≈ 3.4 .

The Cu and O Knight shifts are shown to have similar T (temperature) dependence to the O relaxation rate although, strictly speaking, we expect deviations to exist. Once again, the above-mentioned reasons for the relaxation rates come into play. Finally, we show that the extra 3D dispersion one expects for these bands in optimally doped $\text{YBa}_2\text{Cu}_3\text{O}_7$ can resolve the lack of T dependence of the Knight shifts and O relaxation rate observed for this cuprate.

With the same parameters, the Hall effect is calculated using standard Bloch-Boltzmann theory and is shown to have the observed monotonic decreasing T dependence varying by $\approx 40\%$ over the temperature range compared to the experimental¹² value of $\approx 50\%$, with absolute values about 13 times larger than measured values.

The linear resistivity is also obtained due to phonon relaxation across the bands. The sensitivity of R_h and ρ to the doping follows naturally from the model. The qualitative features of the above experiments are straightforward from the considerations presented here. These features are very robust and do not depend sensitively at all on the choice of parameters used. This is particularly gratifying because these features are observed for a variety of different materials. Derivations of so many of the anomalous normal-state properties of the cuprates lends confidence to the overall theory.

Section II motivates and defines the IBP model. A Hamiltonian is written down and solved within the BCS mean-field approximation. The orbital character of our bands is chosen. The optimal doping for superconductivity as the Fermi-surface touching point is discussed. The lack of a unique phase for the attractive coupling matrix element $V_{kk'}$ is discussed and the difference between Josephson tunneling in standard BCS-like intraband pairing and IBP schemes is derived. IBP due to coupling through phonons is proposed. Up to this point the arguments and equations presented in Sec. II are quite general. There are several different channels through which IBP could occur. One particular channel is chosen and we restrict ourselves to singlet pairs only. There is nothing in the general theory that precludes IBP due to phonons with triplet pairs as far as we can see.

The four key Josephson tunneling experiments^{2,3,13,14} are discussed. We show that with our choice of pairing channel, the two “ d -wave” results of Wollman *et al.*² and Tsuei *et al.*³ can be understood. Our theory also predicts “ d -wave” in contrast to the observed c -axis tunneling of Sun *et al.*¹³ We are unable at present to decide whether the “ s -wave” result of Chaudhari and Lin¹⁴ supports or contradicts our model due to the complexity of the single-particle tunneling

matrix elements in this case. Section III presents quantitative calculations of the various normal-state properties mentioned above and the final section is devoted to a summary of our results.

II. INTERBAND PAIRING MODEL

A. The model

The T_c of the cuprates is quite sensitive to the doping. Typically, there exists one optimal doping¹⁵ for the highest T_c and a rapid change in T_c above and below this doping. A notable exception is Y-Ba-Cu-O,¹⁶ where one may argue that there are two optimal dopings, $T_c = 62, 92$ K with an intermediate crossover regime. An explanation for two T_c regimes in Y-Ba-Cu-O is discussed using IBP in the following paper.⁴ Regardless, whether we argue for one or two optimal dopings for Y-Ba-Cu-O, it is natural to associate the change in T_c with doping to an attractive coupling that is strongly doping dependent. Experimentally,¹⁷ many normal-state properties are simultaneously strongly dependent on the doping. Thus, one is led to propose a bosonic excitation that couples to the electronic charge where either (or both) the bosons or their electronic coupling is strongly renormalized by the doping level. Rather than such dynamic schemes for the change in the attractive coupling with doping, we ask if there exists a simple kinematic scheme for the doping dependence of T_c . In such a scheme, we hope to find a pairing strength that weakly depends on doping with the suppression of T_c due primarily to a kinematic mechanism. IBP is such a mechanism.

Consider two bands labeled U and L with dispersions $\epsilon_k^{(U)}$, $\epsilon_k^{(L)}$ and further suppose there exists some attractive coupling leading to Cooper pairs of the form $(k_U \uparrow, -k_L \downarrow)$ and $(k_L \uparrow, -k_U \downarrow)$. In general, $\epsilon_k^{(U)} \neq \epsilon_k^{(L)}$. It is only when $\epsilon_k^{(U)}$ and $\epsilon_k^{(L)}$ are both close to the Fermi energy that there is any possibility of a lowering of the overall energy by the formation of a Cooper pair. In BCS superconductors, pairs are formed for k states satisfying

$$|\epsilon_k - \epsilon_F| < \hbar \omega_D, \quad (1)$$

where $\hbar \omega_D$ is the Debye energy and ϵ_F is the Fermi energy. For IBP, the analogous criteria are

$$|\epsilon_k^{(U)} - \epsilon_F| < \hbar \omega_D, \quad (2)$$

$$|\epsilon_k^{(L)} - \epsilon_F| < \hbar \omega_D. \quad (3)$$

For BCS superconductors, there are always k states in the required energy range for pairing regardless of the doping. This is no longer the case for IBP because Eqs. (2) and (3) must both be satisfied. It is only for special dopings that the U band and L band Fermi surfaces touch or are close to touching that any possibility exists for IBP. Hence, with IBP the doping sensitivity of T_c can be understood quite simply as due to the change in the minimal separation in k space of the U and L band Fermi surfaces. No change in the strength of the pair attraction is required. In effect, we have replaced

the requirement of a doping-dependent pairing interaction by a geometric argument based upon the band energy differences in k space.

Away from the band crossing point where Eqs. (2) and (3) cannot both be satisfied, we expect BCS-like pairs to be formed. These will couple to the interband pairs. This recovers the full phase space near the Fermi surface for pairing. Here we consider only the IBP to IBP coupling.

We will of course, take the mediator of the interband attraction to be phonons as in BCS. Because our pairs are comprised of electrons from two bands, the standard arguments for an upper bound of $T_c \approx 30$ K do not apply. This is certainly gratifying as it does not exclude IBP with phonons as a theory for high-temperature superconductors. At present we have no estimate for the expected range of values for T_c with our mechanism.

There are some important differences between the pairing terms in the interband Hamiltonian and a BCS Hamiltonian. In order to highlight these differences we will briefly rederive some of the well-known aspects of the BCS Hamiltonian in order to both generalize to IBP and to establish our notation.

In general, spin is conserved. Thus, there are two kinds of scatterings of BCS-like $(k, -k)$ pairs: singlet to singlet, and triplet to triplet. Let the matrix elements for scattering a $(k, -k)$ singlet (triplet) to a $(k', -k')$ singlet (triplet),

$$\begin{aligned} & \frac{1}{\sqrt{2}} (\phi_k \phi_{-k} \pm \phi_{-k} \phi_k) \frac{1}{\sqrt{2}} (\uparrow\downarrow \mp \downarrow\uparrow) \\ & \rightarrow \frac{1}{\sqrt{2}} (\phi_{k'} \phi_{-k'} \pm \phi_{-k'} \phi_{k'}) \frac{1}{\sqrt{2}} (\uparrow\downarrow \mp \downarrow\uparrow) \end{aligned} \quad (4)$$

be $V_{k'k}^0$ ($V_{k'k}^1$). ϕ_k is a single-particle wave function of momentum k . The first important point is that although ϕ_k is uniquely defined only up to a phase $\phi_k \rightarrow e^{i\theta(k)} \phi_k$, with $\theta(-k) = -\theta(k)$, $V_{k'k}^{0,1}$ is uniquely defined due to the time-reversal invariance of a pair with itself.

The Hamiltonian being Hermitian means $V_{k'k}^{0,1} = V_{kk'}^{0,1*}$ and the time-reversal invariance of H implies $V_{k'k}^{0,1} = V_{kk'}^{0,1}$. Thus, $V_{k'k}^{0,1}$ is always real. In second quantized form,

$$\begin{aligned} & \frac{1}{\sqrt{2}} (\phi_k \phi_{-k} \pm \phi_{-k} \phi_k) \frac{1}{\sqrt{2}} (\uparrow\downarrow \mp \downarrow\uparrow) \\ & = \frac{1}{\sqrt{2}} (a_{k\uparrow}^\dagger a_{-k\downarrow}^\dagger \mp a_{k\downarrow}^\dagger a_{-k\uparrow}^\dagger), \end{aligned} \quad (5)$$

where $a_{k\sigma}^\dagger$ is the creation operator for an electron in state ϕ_k with spin σ . The general pair-pair interaction is

$$\begin{aligned} & \sum_{k'k} V_{k'k}^1 \left\{ \frac{1}{2} (a_{k'\uparrow}^\dagger a_{-k'\downarrow}^\dagger + a_{k'\downarrow}^\dagger a_{-k'\uparrow}^\dagger) (a_{-k\downarrow} a_{k\uparrow} + a_{-k\uparrow} a_{k\downarrow}) + a_{k'\uparrow}^\dagger a_{-k'\uparrow}^\dagger a_{-k\uparrow} a_{k\uparrow} + a_{k'\downarrow}^\dagger a_{-k'\downarrow}^\dagger a_{-k\downarrow} a_{k\downarrow} \right\} \\ & + \sum_{k'k} V_{k'k}^0 \left(\frac{1}{2} (a_{k'\uparrow}^\dagger a_{-k'\downarrow}^\dagger - a_{k'\downarrow}^\dagger a_{-k'\uparrow}^\dagger) (a_{-k\downarrow} a_{k\uparrow} - a_{-k\uparrow} a_{k\downarrow}) \right), \end{aligned} \quad (6)$$

which can be expressed as

$$\begin{aligned} & \sum_{k'k} V_{k'k} a_{k'\uparrow}^\dagger a_{-k'\downarrow}^\dagger a_{-k\downarrow} a_{k\uparrow} \\ & + \sum_{\substack{k'k \\ \sigma}} \frac{1}{4} (V_{k'k} - V_{k'-k}) a_{k'\sigma}^\dagger a_{-k'\sigma}^\dagger a_{-k\sigma} a_{k\sigma}, \end{aligned} \quad (7)$$

where

$$\begin{aligned} V_{k'k} &= \frac{1}{2} [(V_{k'k}^0 + V_{-k'-k}^0 + V_{k'-k}^0 + V_{-k'-k}^0) \\ & + (V_{k'k}^1 + V_{-k'-k}^1 - V_{k'-k}^1 - V_{-k'-k}^1)]. \end{aligned} \quad (8)$$

From the relations for $V_{k'k}^{0,1}$, we have $V_{k'k} = V_{kk'}$ in general, and $V_{k'k} = V_{k'-k}$ for pure singlet pairing, and $V_{k'k} = -V_{k'-k}$ for pure triplet pairing. Finally, $V_{k'k}$ is always real and uniquely defined. For phonon coupling, $V_{k'k}$ is constant leading to pure singlet pairs. The symmetry of $V_{k'k}$ determines the total spin of the Cooper pairs in BCS. This is not true for IBP.

For IBP, let the matrix elements for the scatterings

$$\begin{aligned} & \frac{1}{\sqrt{2}} (\phi_{Uk} \phi_{L-k} \pm \phi_{L-k} \phi_{Uk}) \frac{1}{\sqrt{2}} (\uparrow\downarrow \mp \downarrow\uparrow) \\ & \rightarrow \frac{1}{\sqrt{2}} (\phi_{Uk'} \phi_{L-k'} \pm \phi_{L-k'} \phi_{Uk'}) \frac{1}{\sqrt{2}} (\uparrow\downarrow \mp \downarrow\uparrow) \end{aligned} \quad (9)$$

be $V_{k'k}^0$, $V_{k'k}^1$. Here, $\phi_{U,Lk}$ are the single electron wave functions for each band with momentum k . In this case $V_{k'k}^{0,1}$ is no longer uniquely defined for a change in the definitions of ϕ_{Uk} and ϕ_{Lk} ,

$$\phi_{Uk} \rightarrow e^{i\theta_U(k)} \phi_{Uk}, \quad (10)$$

$$\phi_{Lk} \rightarrow e^{i\theta_L(k)} \phi_{Lk}, \quad (11)$$

where $\theta_{U,L}(-k) = -\theta_{U,L}(k)$ implies

$$V_{k'k}^{0,1} \rightarrow e^{-i[\theta_U(k') - \theta_L(k')]} e^{i[\theta_U(k) - \theta_L(k)]} V_{k'k}^{0,1}. \quad (12)$$

The Hermiticity implies, $V_{k'k}^{0,1} = V_{kk'}^{0,1*}$ and time-reversal symmetry leads to $V_{k'k}^{0,1} = V_{-k-k'}^{0,1}$ rather than $V_{k'k}^{0,1} = V_{kk'}^{0,1}$ for BCS. This is due to interband Cooper pairs not being time-reversal invariant with themselves.

The general pair-pair interband pairing interaction is

$$\begin{aligned} & \sum_{k'k} V_{k'k}^1 \left\{ \frac{1}{2} (a_{Uk'\uparrow}^\dagger a_{L-k'\downarrow}^\dagger + a_{Uk'\downarrow}^\dagger a_{L-k'\uparrow}^\dagger) (a_{L-k\downarrow} a_{Uk\uparrow} + a_{L-k\uparrow} a_{Uk\downarrow}) + a_{Uk'\uparrow}^\dagger a_{L-k'\uparrow}^\dagger a_{L-k\uparrow} a_{Uk\uparrow} + a_{Uk'\downarrow}^\dagger a_{L-k'\downarrow}^\dagger a_{L-k\downarrow} a_{Uk\downarrow} \right\} \\ & + \sum_{k'k} V_{k'k}^0 \left(\frac{1}{2} (a_{Uk'\uparrow}^\dagger a_{L-k'\downarrow}^\dagger - a_{Uk'\downarrow}^\dagger a_{L-k'\uparrow}^\dagger) (a_{L-k\downarrow} a_{Uk\uparrow} - a_{L-k\uparrow} a_{Uk\downarrow}) \right). \end{aligned} \quad (13)$$

These equations make it clear that one cannot even speak of the symmetry of the pairing $V_{k'k}$ without first specifying the phase convention on the single-particle orbitals. Secondly, say we found a phase convention such that $V_{k'k}^{0,1}$ is pure s -wave. Unlike BCS phonon pairing, IBP does not preclude triplet pairing due to phonons. Experimentally, pure triplet pairs are not consistent with the observed Josephson tunneling between a BCS superconductor and the cuprates. There must be some singlet pairs for tunneling to occur. This does not exclude the possibility of some pairs being triplet paired, though. For the rest of this paper however, we will only consider the case of pure singlet pairs, i.e., $V_{k'k}^1 = 0$.

The IBP Hamiltonian becomes

$$\begin{aligned} H = & \sum_{k\sigma} [\epsilon_k^{(U)} a_{Uk\sigma}^\dagger a_{Uk\sigma} + \epsilon_k^{(L)} a_{Lk\sigma}^\dagger a_{Lk\sigma}] \\ & + \sum_{k'k} \frac{1}{2} V_{k'k} (a_{Uk'\uparrow}^\dagger a_{L-k'\downarrow}^\dagger - a_{Uk'\downarrow}^\dagger a_{L-k'\uparrow}^\dagger) \\ & \times (a_{L-k\downarrow} a_{Uk\uparrow} - a_{L-k\uparrow} a_{Uk\downarrow}), \end{aligned} \quad (14)$$

where we write $V_{k'k} = V_{k'k}^0$ for simplicity.

In the pairing approximation, we consider excitations of the form,

$$\psi_0(k) = (u_k + v_k a_{Uk\uparrow}^\dagger a_{L-k\downarrow}^\dagger) |0\rangle, \quad (15)$$

$$p_0(k) = (1 - f_k^{(U)})(1 - f_k^{(L)}),$$

$$\psi_1(k) = a_{Uk\uparrow}^\dagger |0\rangle, \quad p_1(k) = f_k^{(U)}(1 - f_k^{(L)}), \quad (16)$$

$$\psi_2(k) = a_{L-k\downarrow}^\dagger |0\rangle, \quad p_2(k) = (1 - f_k^{(U)})f_k^{(L)}, \quad (17)$$

$$\psi_3(k) = (-v_k + u_k a_{Uk\uparrow}^\dagger a_{L-k\downarrow}^\dagger) |0\rangle, \quad p_3(k) = f_k^{(U)}f_k^{(L)}, \quad (18)$$

$$|u_k|^2 + |v_k|^2 = 1 \quad (19)$$

with probabilities $p_i(k)$ where $f_k^{(U)}$ and $f_k^{(L)}$ are the occupation numbers of U and L band particles of momentum k . There are four other excitations ψ_4, \dots, ψ_7 obtained from the above by replacing $a_{Uk\uparrow}^\dagger a_{L-k\downarrow}^\dagger$ with $a_{L-k\uparrow}^\dagger a_{Uk\downarrow}^\dagger$ in ψ_0 and ψ_3 , $a_{Uk\uparrow}^\dagger$ with $a_{L-k\uparrow}^\dagger$ in ψ_1 and $a_{L-k\downarrow}^\dagger$ with $a_{Uk\downarrow}^\dagger$ in ψ_2 . The ordering of the creation operators is chosen such that Cooper pairs consist only of singlet pairs.

The coefficients u_k and v_k are chosen to minimize the free energy $F = H - \mu N - TS$. The solution is

$$|u_k|^2 = 1 - |v_k|^2 = \frac{1}{2} \left(1 + \frac{\xi_k}{E_k} \right), \quad u_k^* v_k = \frac{\Delta_k}{2E_k}, \quad (20)$$

$$\xi_k = \omega_k - \mu, \quad \omega_k = \frac{1}{2} (\epsilon_k^{(U)} + \epsilon_k^{(L)}), \quad (21)$$

$$E_k = \sqrt{\xi_k^2 + |\Delta_k|^2}, \quad (22)$$

$$E_k^{(U)} = \frac{1}{2} [\epsilon_k^{(U)} - \epsilon_k^{(L)}] + E_k, \quad (23)$$

$$E_k^{(L)} = -\frac{1}{2} [\epsilon_k^{(U)} - \epsilon_k^{(L)}] + E_k, \quad (24)$$

$$f_k^{(U)} = \frac{1}{e^{\beta E_k^{(U)}} + 1}, \quad f_k^{(L)} = \frac{1}{e^{\beta E_k^{(L)}} + 1}, \quad (25)$$

with gap equation

$$\Delta_k = \sum_{k'} V_{kk'} \frac{\Delta_{k'}}{2E_{k'}} (1 - f_{k'}^{(U)} - f_{k'}^{(L)}). \quad (26)$$

Conservation of the total number of particles N leads to an equation for the chemical potential μ

$$N = \sum_k 2|v_k|^2 (1 - f_k^{(U)} - f_k^{(L)}) + (f_k^{(U)} + f_k^{(L)}). \quad (27)$$

Unlike BCS, the quasiparticle excitation energies are different for the U and L particles and are given by $E_k^{(U)}$ and $E_k^{(L)}$. These energies are the sum of half the difference in the U and L band energies and the term E_k which is analogous to the BCS quasiparticle energy. The most important point of all is that, although the sum $E_k^{(U)} + E_k^{(L)} = 2E_k$ is always positive, the U or L excitation energy can be negative or have lower energy than the gap energy Δ . This piece of physics will be considered in more detail below.

Also, the BCS quasiparticle energy E_k is formed from a band ω_k that is the mean of the U and L bands. One can see why this is the case by noting that in the BCS ground state, pairs are either fully occupied or completely unoccupied. The individual band energies always appear summed together, $\epsilon_k^{(U)} + \epsilon_k^{(L)} = 2\omega_k$. For these states, the system ‘‘does not know’’ that the U and L pairing electrons have different energies. The three equations for the pair occupation amplitudes u_k and v_k , incorporate the difference between the two-band dispersions only through the gap Δ_k . This is to be expected by the same argument as above because u_k and v_k represent pair occupations. Similarly, the gap equation incorporates the U and L band differences through the quasiparticle occupation numbers, $f^{(U)}$ and $f^{(L)}$.

Looking at the expressions for the quasiparticle excitation energies $E_k^{(U)}$ and $E_k^{(L)}$, one sees that the size of the differ-

ence in energies of the two bands $\epsilon_k^{(U)} - \epsilon_k^{(L)}$ is what determines the size of the excitation. A negative energy implies that no Cooper pair is formed at $T=0$. Instead, there is a single free electron in one band and no electron in the other. When $\epsilon_k^{(U)} - \epsilon_k^{(L)}$ is large, it is energetically unfavorable to occupy both k states or empty both k states. Thus no pair is formed. In this case, we expect BCS-like pairs to be formed. Near a Fermi-surface touching point, $\epsilon_k^{(U)} \approx \epsilon_k^{(L)}$. Therefore, interband pairs are always energetically favored.

These equations are very similar to the equations for gapless superconductivity.¹⁸ In gapless superconductivity, an \uparrow spin electron has a slightly different dispersion than the \downarrow spin electrons due to the presence of magnetic impurities. These \uparrow and \downarrow spin bands are analogous to the U and L bands in IBP.

B. The two relevant bands

Perry and Tahir-Kheli⁴ have calculated *ab initio* the existence of two bands near the Fermi energy for $\text{La}_{1.85}\text{Sr}_{0.15}\text{CuO}_4$. The results of that work are briefly summarized in this subsection.

La_2CuO_4 has two structural phases: a high-temperature body-centered-tetragonal crystal with D_{4h} point group and a low-temperature orthorhombic lattice with C_{2h} point group. In the low-temperature phase, the CuO_6 octahedra are tipped by 4.3° from their high-temperature positions thereby reducing the symmetry of the crystal. The low-temperature phase is the structure for superconductivity. In the tetragonal crystal, there are two reflection planes defined by the z axis and the lines $x=y$ and $x=-y$, respectively. For the orthorhombic crystal, there is only one reflection plane defined by the z axis and $x=y$.

In either case, there will be a rigorous band crossing along $k_x=k_y$ for our two bands. The tetragonal phase will also have a crossing along $k_x=-k_y$. The orthorhombic phase will come close to crossing along $k_x=-k_y$, but cannot cross. For IBP to occur, it is imperative that a crossing exist, otherwise it is hard to see how IBP can overcome the band repulsion. For the remainder of this paper and in the following paper, we will take the La-Sr-Cu-O crystal structure to be the high-temperature tetragonal phase for simplicity. The small difference in structures can have a big effect on T_c , but for most normal state properties, the difference will be small.

In undoped La_2CuO_4 , the O sites have a formal charge of -2 , the Cu charge is $+2$ and is in a d^9 state. The point charge field on the Cu site due to the surrounding atoms make the $d_{x^2-y^2}$ orbital the most unstable leading to holes in this orbital in the undoped system. The next highest (unstable) orbital on the Cu is d_{z^2} due to the field of the apical oxygens. Undoped, each Cu $d_{x^2-y^2}$ has a single electron and d_{z^2} has 2 electrons. We propose that as the system is doped

to its metallic/superconducting phase, holes start to appear in the Cu d_{z^2} orbital. At an arbitrary k point in the Brillouin zone, d_{z^2} can mix with $d_{x^2-y^2}$, O p_σ , and apical O p_z orbitals. Thus, the two relevant bands at the Fermi energy are comprised primarily of these four orbitals.

This assumption of the existence of d_{z^2} holes near the Fermi energy along with the assumption of interband pairing must be regarded as the two most important postulates of the IBP model for the cuprates. The former postulate is discussed in detail using *ab-initio* calculations on small clusters in the following paper⁴ where we conclude that there are two bands near the Fermi energy with the character described above.

We will call the two bands the upper (U) and lower (L) bands where $\epsilon_k^{(U)} \geq \epsilon_k^{(L)}$. The lower band should be full or almost full in the undoped case and the upper band is half full with all of its holes predominantly of $d_{x^2-y^2}$ character. For La-Sr-Cu-O, the U and L bands will be almost completely 2D, while for optimally doped $\text{YBa}_2\text{Cu}_3\text{O}_7$, the bands will have a measurable amount of 3D character. Underdoped $\text{YBa}_2\text{Cu}_3\text{O}_{6.63}$ will have less 3D dispersion than optimally doped $\text{YBa}_2\text{Cu}_3\text{O}_7$ (YBCO). Additionally, for YBCO there are potentially four relevant bands due to the two CuO planes per unit cell. Here, we restrict our attention to La-Sr-Cu-O and briefly discuss the differences to expect for YBCO where appropriate.

The unit cell of two formula units of La_2CuO_4 is tetragonal with lattice spacing $a=4.0 \text{ \AA}$ in the x, y directions and $c=12.0 \text{ \AA}$ in the z direction. The Brillouin zone of the primitive unit cell is given by $-\pi/a \leq k_x \leq \pi/a$, $-\pi/a \leq k_y \leq \pi/a$, $-2\pi/c \leq k_z \leq 2\pi/c$.

To a first approximation, we may take the U and L bands for La-Sr-Cu-O to be purely 2D and add in the weak z -axis dispersion as a first-order perturbation. This is done primarily for further computational simplicity and to convey the key aspects of the model. A more correct description will not qualitatively alter the behaviors we obtain for the NMR and Hall effect and more importantly, will not affect the general arguments for the various normal-state properties.

The relevant orbitals are d_{z^2} , $d_{x^2-y^2}$ on the Cu, p_σ orbitals on the two planar O sites (σ along the CuO bond direction), and p_z orbitals for the two apical O sites above and below the Cu atom. Additional orbitals that appear are the Cu $4s$, d_{xy} , and O p_π in the plane and the p_x, p_y orbitals on the apical O's. None of these additional orbitals will lead to a big change in the band structure but can affect the NMR. In particular, a small amount of Cu $4s$ is required for an understanding of the sign of the Knight shift on Cu and some (a few percent) d_{xy} is necessary for explaining the large anisotropy in the Cu spin-relaxation rates for planar and z -axis magnetic fields.

The tight-binding Hubbard model is (we use the electron picture),

$$H = H_{\text{orb}} + H_{\text{hop}}, \quad (28)$$

$$H_{\text{orb}} = \sum_{n\sigma} \epsilon_{d_{x^2-y^2}} d_{x^2-y^2 n\sigma}^\dagger d_{x^2-y^2 n\sigma} + \epsilon_{d_{z^2}} d_{z^2 n\sigma}^\dagger d_{z^2 n\sigma} + \sum_{n\sigma} \epsilon_{p_\sigma} (p_{xn\sigma}^\dagger p_{xn\sigma} + p_{yn\sigma}^\dagger p_{yn\sigma}) + \epsilon_{p_z} (p_{Uzn\sigma}^\dagger p_{Uzn\sigma} + p_{Lzn\sigma}^\dagger p_{Lzn\sigma}), \quad (29)$$

$$\begin{aligned}
H_{\text{hop}} = & \pm t_{x^2-y^2, \sigma} \sum_{\langle nm \rangle} d_{x^2-y^2 n \sigma}^\dagger (p_{xm \sigma} + p_{ym \sigma}) \pm t_{z^2, \sigma} \sum_{\langle nm \rangle} d_{z^2 n \sigma}^\dagger (p_{xm \sigma} + p_{ym \sigma}) \\
& + (\pm t_{\sigma \sigma}) \sum_{\langle nm \rangle} p_{xn \sigma}^\dagger p_{ym \sigma} + (\pm t_{p_z, d_z^2}) \sum_{n \sigma} d_{z^2 n \sigma}^\dagger (p_{zU n \sigma} - p_{zL n \sigma}) + t_{p_z, p_z} \sum_{n \sigma} p_{zU n \sigma}^\dagger p_{zL n \sigma} \\
& + (\pm t_{\sigma \sigma a}) \sum_{\substack{\langle nm \rangle \sigma \\ \text{same} \\ \text{axis}}} (p_{xn \sigma}^\dagger p_{xm \sigma} + p_{yn \sigma}^\dagger p_{ym \sigma}) + (\pm t_{p_z, \sigma}) \sum_{\langle nm \rangle} (p_{zU n \sigma}^\dagger - p_{zL n \sigma}^\dagger) (p_{xm \sigma} - p_{ym \sigma}) + \text{c.c.}, \quad (30)
\end{aligned}$$

where $d_{z^2 n \sigma}^\dagger$ creates a d_{z^2} orbital with spin σ at site n . $p_{xn \sigma}^\dagger$ ($p_{yn \sigma}^\dagger$) creates a p_σ electron on a planar O site along the x (y) axis and $p_{zU n \sigma}^\dagger$ ($p_{zL n \sigma}^\dagger$) creates a p_z electron on the apical O site above (below) the CuO plane. $\epsilon_{d_z^2}$ is the self (orbital) energy of the d_{z^2} , etc. The t 's are the various hopping matrix elements. The \pm sign in front of the hopping matrix elements represents the fact that the sign of the matrix element depends on the relative position of the two relevant orbitals. $\langle nm \rangle$ represents neighboring sites. The values of the parameters are shown in Table I. The values in Table I for the hopping t 's are for the antibonding combination of the two relevant orbitals.

Except for the value of the difference $\epsilon_{d_z^2} - \epsilon_{d_{x^2-y^2}}$, there is nothing particularly surprising or out of the ordinary with these parameters. $\epsilon_{d_z^2} - \epsilon_{d_{x^2-y^2}}$ being positive is what brings the d_{z^2} orbital up to the Fermi energy. This is the essential parameter for a two-band description (like ours) of superconductivity. These points are discussed in detail in the following paper⁴ where our parameters are derived from *ab initio* calculations on small clusters. As we stated in the introduction, the theory presented here is very robust and at a qualitative level does not depend sensitively on the values for these parameters at all.

The point group of La-Sr-Cu-O is D_{4h} and $d_{x^2-y^2}$, d_{z^2} transform as B_{1g} and A_{1g} , respectively. Under a σ_d reflection about the diagonals $x = \pm y$, $\sigma_d d_{x^2-y^2} = -d_{x^2-y^2}$ and $\sigma_d d_{z^2} = d_{z^2}$. Thus, for diagonal k vectors ($k_x = \pm k_y$) a single electron wave function must have $d_{x^2-y^2}$ character or d_{z^2} character. Along $k_x = \pm k_y$, two bands may cross if one band has $d_{x^2-y^2}$ character and the other has d_{z^2} character. A plot of the top two bands (most unstable) is shown in Fig. 1 along the closed path $(0,0) - (\pi, \pi) - (\pi, 0) - (0,0)$ in k space. For

TABLE I. Parameters in Hubbard model in (eV).

$\epsilon_{d_{x^2-y^2}}$	-2.403
$\epsilon_{d_{z^2}}$	-2.092
ϵ_{p_σ}	-6.122
ϵ_{p_z}	-0.852
$t_{x^2-y^2, \sigma}$	1.347
$t_{z^2, \sigma}$	0.514
$t_{\sigma \sigma}$	0.368
$t_{\sigma \sigma a}$	-0.041
t_{p_z, d_z^2}	1.076
$t_{p_z, \sigma}$	0.078
t_{p_z, p_z}	0.493

all k points not on the diagonal, there is no symmetry to keep $d_{x^2-y^2}$ and d_{z^2} from mixing. Thus, the two bands will repel leading to $\epsilon_k^{(U)} > \epsilon_k^{(L)}$.

The optimal doping for the highest T_c is the doping that leads to a Fermi energy equal to the energy at the band crossing or touching point. It is at this doping and this doping only that there is favorable energetics for interband pair formation. Figure 2 shows the Fermi surface at various doping from underdoped to overdoped.

We have adjusted the charge transfer of planar O p_π onto the La described in detail in the following paper⁴ such that this doping matches the experimentally observed optimal doping for $\text{La}_{2-x}\text{Sr}_x\text{CuO}_4$ at $x=0.15$. Undoped, there are a total of three electrons in the U and L bands, while for $x=0.15$ there are $3 - 0.15 = 2.85$ electrons in the two bands.

The z -axis (normal to the CuO planes) dispersion is approximately calculated by observing that the dominant coupling in the z direction is the p_z orbital on the apical O above a CuO plane coupling to the p_z orbital on the apical O below the next higher CuO plane. We take this value to be $T_{(0,0)} = 0.3$ eV. The coupling is added in via first-order perturbation theory. Our choice for this matrix element is described below.

The additional energy of a k state due to p_z to p_z coupling from layer to layer is

$$\epsilon(k_x, k_y, k_z) = -2T_{(0,0)}P \cos \frac{1}{2}(k_x a) \cos \frac{1}{2}(k_y a) \cos k_z c, \quad (31)$$

where P is the amount of apical O p_z character in the k state (k_x, k_y) derived from the 2D Hamiltonian (28).

To incorporate the very small couplings through the p_x

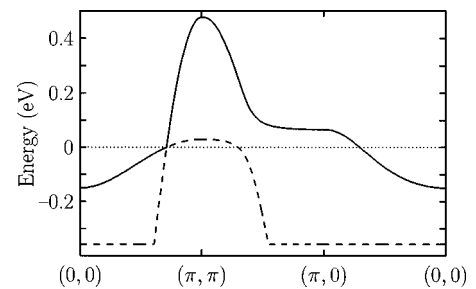


FIG. 1. Dispersions of the U (solid line) and L (dashed line) bands.

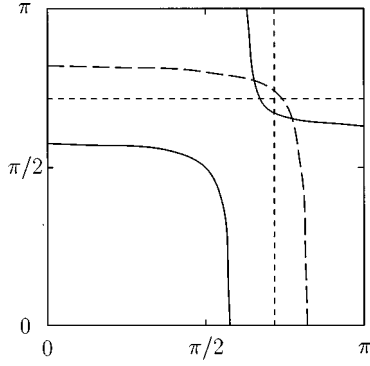


FIG. 2. Fermi surfaces at various dopings. The short dashes are for optimal doping, the long dashes are underdoping, and the solid line is overdoping.

and p_y orbitals on the apical O above a CuO plane with the p_z on the apical O below the next higher plane, an additional energy

$$\begin{aligned} \epsilon(k_x, k_y, k_z) = & -2T_{(\pi,0)}P \left[\cos \frac{1}{2}(k_x a) \sin \frac{1}{2}(k_y a) \right. \\ & \left. + \sin \frac{1}{2}(k_x a) \cos \frac{1}{2}(k_y a) \right] \cos k_z c, \quad (32) \end{aligned}$$

is added. Finally, we add

$$\epsilon(k_x, k_y, k_z) = -2T_{(\pi,\pi)}P \sin \frac{1}{2}(k_x a) \sin \frac{1}{2}(k_y a) \cos k_z c, \quad (33)$$

to include the weak coupling of Cu d_{xy} with apical O p_z . We take $T_{(\pi,0)} = 0.05$ eV, $T_{(\pi,\pi)} = 0.02$ eV.

The reason for naming the hopping matrix elements with the k -space labels $(0,0)$, $(\pi,0)$, (π,π) is that each one is multiplied by a combination of $\cos(1/2)k_x a$, $\cos(1/2)k_y a$, $\sin(1/2)k_x a$, $\sin(1/2)k_y a$ which is equal to 1 on the particular k -space label and zero at the other two. We expect $T_{(0,0)} > T_{(\pi,0)} > T_{(\pi,\pi)}$.

The primary effect of adding in the above z -axis couplings is to eliminate the logarithmic 2D van Hove saddle-point singularity in the density of states of the U band by a broadened 3D peak. The width of this peak is responsible for the T dependence (or lack thereof in $\text{YBa}_2\text{Cu}_3\text{O}_7$) of the Knight shifts in the normal state. This is shown further along in the calculation of the NMR.

Figure 3 shows the density of states of the two bands with

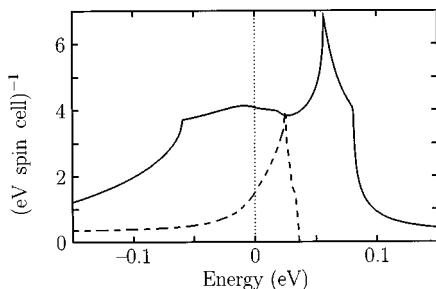


FIG. 3. Density of states of the U (solid line) and L (dashed line) bands near the optimal Fermi energy. The density units are states per eV per spin per unit cell.

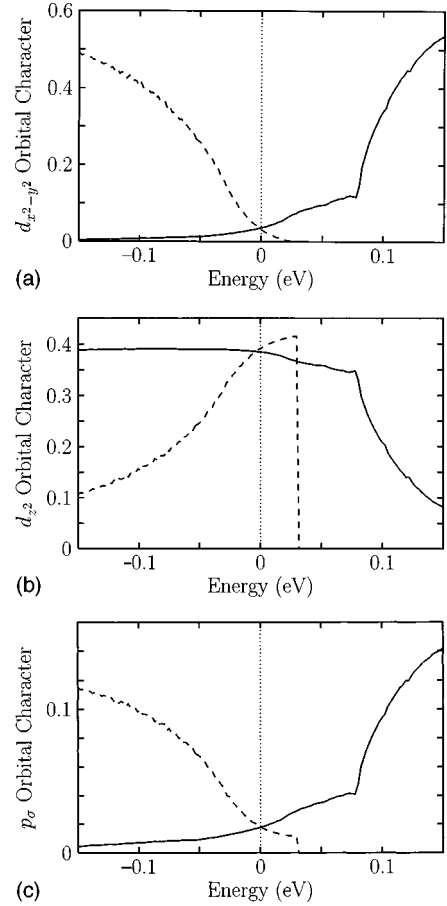


FIG. 4. Orbital characters of the U (solid line) and L (dashed line) bands. (a) is the $d_{x^2-y^2}$ character, (b) is the d_{z^2} character, and (c) is the p_{σ} character.

the Fermi energy at the optimal doping indicated. The large peak in the U band density of states just above the optimal doping Fermi energy $\epsilon_F = 0.0$ eV is due to the saddle-point singularity at $(\pi,0)$ and $(0,\pi)$. The closeness of this peak to ϵ_F is a robust feature of this model and is not sensitive to the choice of parameters.

Three other features of interest are shown in Figs. 4(a)–4(c). They show the average amount of $d_{x^2-y^2}$, d_{z^2} , and p_{σ} character of the two bands at different energies. Near ϵ_F , the two bands are predominantly d_{z^2} . Both of these features are once again robust.

C. The pairing term

There are several different choices for the detailed orbital coupling that can lead to IBP. Lacking a rigorous microscopic proof that IBP exists, we make a particular choice for the pairing term and compare it to experiment. We take the pairing term in Eq. (14) to be mediated by an attractive coupling of the form shown in Fig. 5. In this figure, $d_{x^2-y^2k}$ and d_{z^2k} are defined as

$$d_{x^2-y^2k}(\mathbf{r}) = \frac{1}{\sqrt{N}} \sum e^{ik \cdot \mathbf{R}} d_{x^2-y^2}(\mathbf{r} - \mathbf{R}), \quad (34)$$

$$d_{z^2k}(\mathbf{r}) = \frac{1}{\sqrt{N}} \sum e^{ik \cdot \mathbf{R}} d_{z^2}(\mathbf{r} - \mathbf{R}), \quad (35)$$

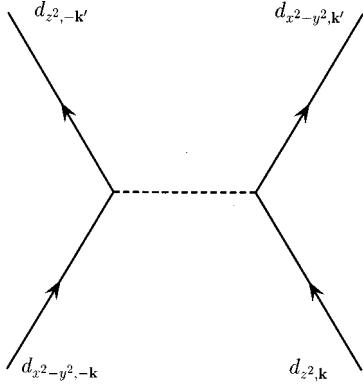


FIG. 5. Feynman diagram for the pairing term with matrix element $U_{k'k}$.

where \mathbf{R} is the position of the Cu atom. Eventually, we will take the origin to be a center of inversion. Figure 5 depicts a $d_{x^2-y^2}$ Bloch orbital of momentum $-k$ emitting a virtual phonon and scattering to a d_{z^2} orbital of momentum $-k'$ and a d_{z^2} orbital of momentum k absorbing the phonon and scattering to a $d_{x^2-y^2}$ orbital of momentum k' . Equations (34) and (35) define the phase convention of the $d_{x^2-y^2}$ and d_{z^2} Bloch functions and the matrix element $U_{k'k}$. The coupling $V_{k'k}$ in Eq. (14) is calculated by projecting onto the above $d_{x^2-y^2}$, d_{z^2} scattering. Physically, what is accomplished is quite straightforward. The attractive coupling between two single-electron states k , $-k$ in the same band or two different bands is due primarily to the attractive coupling of the $d_{x^2-y^2}$ orbital component of one electron with the d_{z^2} component of the other electron. One reason that such a coupling may arise is from the dynamic Jahn-Teller effect which acts to split the orbital degeneracy at the crossing point. Another reason is due to the $d_{x^2-y^2}$ k states localizing the electron charge in the plane, whereas the d_{z^2} $-k$ state localizes the charge out of the CuO plane thereby reducing the Coulomb repulsion.

An attractive coupling mediated by projection onto the diagram in Fig. 5 is also possible for $(k\uparrow, -k\downarrow)$ pairs in the same band leading to a traditional BCS pairing term. Thus, one is faced with the possibility that BCS-like intraband pairing may win out over IBP. This possibility is not realized for k states near the band crossing point by the same kinematics that allows a band crossing to occur along the diagonals ($k_x = \pm k_y$). In order to have a large BCS-like pairing for a Cooper pair $(k\uparrow, -k\downarrow)$ in the same band with a k state near the crossing point one requires a substantial amount of both $d_{x^2-y^2}$ and d_{z^2} in the k state. Near the band crossing point, the approximate σ_d diagonal reflection symmetry precludes that leading to a suppression of BCS-like pairing by the above pairing mechanism. Also, because the U and L k states are almost degenerate here, the system may further lower its energy by forming a pure $d_{x^2-y^2}$ and a pure d_{z^2} state in order to maximize the pairing coupling. Such states should be considered as vibronic. At k points away from the diagonals, BCS-like pairing can occur and for arbitrary dopings, too.

Including BCS-like intraband pairing by projection of Fig. 5 as we did for IBP is straightforward. Rather than diagonalizing a 2×2 matrix as we did in deriving Eqs. (15)–(27), we

must diagonalize a 4×4 matrix. This is not difficult to do and leads to more complicated quasiparticle energies than Eqs. (23) and (24). To properly include BCS-like pairs, we should not restrict ourselves to the single diagram in Fig. 5. There are other combinations of interband to BCS-like pair scatterings that may become important.

Physically, what occurs is near the band crossing point on the diagonals, interband pairs are formed because one band is almost pure $d_{x^2-y^2}$ (with some O character) and the other band is almost pure d_{z^2} (again with O character). Away from the Fermi-surface touching point, only BCS-like pairs are kinematically allowed leading to standard BCS pairs for the k states. Thus, one would expect to observe a gap in the photoemission for k vectors away from the diagonal as is observed¹⁹ for angle-resolved photoemission on bismuth 2212. We also find that the pseudogap²⁰ behavior can be explained by IBP and our calculated band structure.²¹

Owing to the separation of the pairs along the diagonal into one band with no $d_{x^2-y^2}$ character and the other with no d_{z^2} character, pairs are most strongly formed here than at any other k point. This suggests that the dominant contribution to the Josephson tunneling current will come from IBP along the diagonals and we assume this is true unless such a current is rigorously zero.

Let

$$\phi_{Uk} = A_{Uk}d_{x^2-y^2k} + B_{Uk}d_{z^2k} + \text{other terms}, \quad (36)$$

$$\phi_{Lk} = A_{Lk}d_{x^2-y^2k} + B_{Lk}d_{z^2k} + \text{other terms}, \quad (37)$$

where ϕ_{Uk} and ϕ_{Lk} are the band wave functions and A_k , B_k are the projections onto the Bloch functions in Eqs. (34), (35). Then,

$$a_{Uk}^\dagger = A_{Uk}d_{x^2-y^2k}^\dagger + B_{Uk}d_{z^2k}^\dagger + \dots, \quad (38)$$

$$a_{Lk}^\dagger = A_{Lk}d_{x^2-y^2k}^\dagger + B_{Lk}d_{z^2k}^\dagger + \dots, \quad (39)$$

and

$$d_{x^2-y^2k}^\dagger = A_{Uk}^* a_{Uk}^\dagger + A_{Lk}^* a_{Lk}^\dagger + \dots, \quad (40)$$

$$d_{z^2k}^\dagger = B_{Uk}^* a_{Uk}^\dagger + B_{Lk}^* a_{Lk}^\dagger + \dots. \quad (41)$$

The pairing Hamiltonian term is

$$U_{k'k}(d_{x^2-y^2k'}^\dagger d_{z^2-k'}^\dagger d_{x^2-y^2-k} d_{z^2k} + d_{x^2-y^2k'}^\dagger d_{z^2-k'}^\dagger d_{x^2-y^2-k} d_{z^2k}). \quad (42)$$

Projecting onto Eq. (14),

$$\begin{aligned} V_{k'k} = & (A_{Uk'} B_{L-k'})^* (A_{Uk} B_{L-k}) U_{k'-k} \\ & + (B_{Uk'} A_{L-k'})^* (B_{Uk} A_{L-k}) U_{-k'k} \\ & + (A_{Uk'} B_{L-k'})^* (B_{Uk} A_{L-k}) U_{k'k} \\ & + (B_{Uk'} A_{L-k'})^* (A_{Uk} B_{L-k}) U_{-k'-k}. \end{aligned} \quad (43)$$

Under the phase change in Eqs. (10) and (11)

$$A_{U,Lk} \rightarrow e^{i\theta_{U,L(k)}} A_{U,Lk}, \quad (44)$$

$$B_{U,Lk} \rightarrow e^{i\theta_{U,L(k)}} B_{U,Lk}, \quad (45)$$

and thus $V_{k'k}$ transforms as Eq. (12).

Now every cuprate space group includes the inversion operator. We define the origin from which \mathbf{R} in Eqs. (34) and (35) is defined as a point of inversion. With this choice it is easy to see that the coefficients $A_{U,Lk}$, $B_{U,Lk}$ must always satisfy $A_k^* B_k = \text{real}$.

In general, the electron-phonon matrix element that appears at each vertex in the Feynman diagram in Fig. 5 is the sum of terms of the form

$$i(\mathbf{e}_{\lambda q} \cdot \mathbf{q}) V_{\lambda q} (c_{q\lambda} + c_{-q\lambda}^\dagger) \int e^{iq \cdot r} d_{x^2-y^2, k'}^*(r) d_{z^2, k}(r) d\tau, \quad (46)$$

where λ is the phonon polarization and \mathbf{q} is its momentum. $c_{q\lambda}$ is the destruction operator and $V_{\lambda q}$ is the Fourier transform of the phonon potential and $\mathbf{e}_{\lambda q}$ is the polarization vector. Inversion symmetry guarantees $V_{\lambda -q} = V_{\lambda q}$, $V_{\lambda q}$ is always real and also that the integral in Eq. (46) over the electron states is real.

Using Eqs. (34) and (35), the integral in Eq. (46) is

$$\begin{aligned} & \int e^{iq \cdot r} d_{x^2-y^2, k'}^*(r) d_{z^2, k}(r) d\tau \\ &= \frac{1}{N} \int e^{iq \cdot r} \sum_{\mathbf{R}\mathbf{R}'} e^{-ik' \cdot \mathbf{R}'} e^{ik \cdot \mathbf{R}} d_{x^2-y^2}(r - \mathbf{R}') d_{z^2}(r - \mathbf{R}). \end{aligned} \quad (47)$$

Taking the largest contribution to be when $\mathbf{R}' = \mathbf{R}$,

$$\int e^{iq \cdot r} d_{x^2-y^2, k'}^*(r) d_{z^2, k}(r) d\tau = \int e^{iq \cdot r} d_{x^2-y^2}(r) d_{z^2}(r) d\tau. \quad (48)$$

Plugging this back into Eq. (46), we see that the product of the two electron-phonon matrix elements due to the two vertices in Fig. 5 is always positive with the phase convention defined in Eqs. (34), (35) where the origin of \mathbf{R} is an inversion center. With BCS-like pairing, time-reversal symmetry of the Cooper pairs is sufficient to guarantee the product of the two vertices is always mod-squared and thus positive.

Therefore, with our definitions of the $d_{x^2-y^2}$, d_{z^2} Bloch functions, we may take the total coupling $U_{k'k}$ from Fig. 5 to be s like,

$$U_{k'k} = \begin{cases} -V, & |\epsilon_k^{(U,L)} - \mu| < \hbar\omega_D \quad \text{and} \quad |\epsilon_{k'}^{(U,L)} - \mu| < \hbar\omega_D, \\ 0, & \text{otherwise,} \end{cases} \quad (49)$$

leading to

$$\begin{aligned} V_{k'k} &= (-V)(A_{Uk'} B_{L-k} + B_{Uk'} A_{L-k'})^* \\ &\quad \times (A_{Uk} B_{L-k} + B_{Uk} A_{L-k}). \end{aligned} \quad (50)$$

The reason we have chosen the above range of k' , k values for nonzero pairing is seen by considering the relevant Feynman diagram in Fig. 5. The value is

$$\begin{aligned} & \frac{1}{2} \left[\frac{1}{[\epsilon_{k'}^{(U)} - \epsilon_k^{(L)}]^2 - \hbar^2 \omega^2} \right. \\ & \quad \left. + \frac{1}{[\epsilon_{k'}^{(L)} - \epsilon_k^{(U)}]^2 - \hbar^2 \omega^2} \right] \cdot (A_{Uk'} B_{L-k} + B_{Uk'} A_{L-k'})^* \\ & \quad \times (A_{Uk} B_{L-k} + B_{Uk} A_{L-k}) M^2, \end{aligned} \quad (51)$$

where M^2 is a real positive number. If the constraints in Eq. (49) are satisfied, then the term in brackets is negative.

D. Interband Josephson tunneling

In BCS theory, a Cooper pair is of the form $\phi_{k\uparrow} \phi_{-k\downarrow}$ and transforms into itself under the operation of time reversal. For pairing across two distinct bands as we propose, the pair $\phi_{Uk\uparrow} \phi_{L-k\downarrow}$ transforms into $\phi_{Lk\uparrow} \phi_{U-k\downarrow}$ and not into itself under time reversal. Of course, the full Hamiltonian remains time-reversal invariant. This key difference alters the standard Josephson tunneling in a subtle yet dramatic way that leads to a new interpretation of the macroscopic phase of superconductors.

Consider first the case of Josephson tunneling of a BCS-like Cooper pair on one side of a junction to a BCS-like pair on the other side of the junction. We will neglect all factors in the expression for the supercurrent J contributing only to the magnitude and not to the phase of J . The phase of the pair tunneling matrix element for the transfer of a $(k\uparrow, -k\downarrow)$ pair to a $(p\uparrow, -p\downarrow)$ pair is contained in the product of two single-electron tunneling matrix elements, T_{kp} and T_{-k-p} and the product of the two gap functions, Δ_k^* and Δ'_p on either side of the junction. This leads to supercurrent¹⁸

$$J \propto T_{kp} T_{-k,-p} \Delta_k \Delta'_p{}^* = |T_{kp}|^2 \Delta_k \Delta'_p{}^*. \quad (52)$$

In this expression, T_{kp} is the matrix element for the transfer of a single electron of momentum k to an electron of momentum p , T_{-k-p} is the corresponding matrix element for transferring the $-k$ electron to $-p$ and Δ_k, Δ'_p are the gap functions on the two sides of the junction. By overall time-reversal symmetry, $T_{-k-p} = T_{kp}^*$. Thus, the supercurrent is completely controlled by the phases of the superconducting gap functions on each side of the junction. The phases of the pairing interactions for each superconductor. Thus, for all BCS-like pairing models, Josephson tunneling gives direct information of the symmetry of the gap.

For IBP, the situation is dramatically different. Suppose we tunnel from an interband superconductor to a BCS superconductor. With Cooper pairing across bands, the matrix element for transferring a momentum k electron in the U band to a momentum p electron on the other side of the junction $T_{kp}^{(U)}$, is different from the matrix element for transferring a $-k$ electron in the L band to a $-p$ electron on the other side of the junction $T_{-k,-p}^{(L)}$. Although, $T_{-k,-p}^{(U)} = T_{kp}^{(U)*}$ and $T_{-k,-p}^{(L)} = T_{kp}^{(L)*}$ by overall time-reversal symmetry, the phase part of the pair transfer-matrix element is of the form

$$J \propto T_{kp}^{(U)} T_{-k,-p}^{(L)} \Delta_k \Delta'_p{}^*. \quad (53)$$

In the case of interband pairing, *the symmetry of the pairing interactions and the orbital character of the band wave func-*

tions both contribute to the overall tunneling phase. Under a redefinition of the single band wave functions (10), (11),

$$T_{kp}^{(U,L)} \rightarrow e^{i\theta_{U,L}(k)} T_{kp}^{(U,L)}, \quad (54)$$

and from the gap equation (26),

$$\Delta_k \rightarrow e^{-i[\theta_U(k) - \theta_L(k)]} \Delta_k, \quad (55)$$

leading to no change in J . Note also that the above result is independent of the phase convention of the band orbitals on the BCS side of the junction because if an electron of momentum p is multiplied by a phase factor $e^{i\theta}$, then the phase of the $-p$ electron is multiplied by $e^{-i\theta}$.

Remember that as we argued in the previous section, we take the dominant supercurrent to be due to the interband Cooper pairs near the diagonal crossing points.

Let us apply our relation (53) for the supercurrent to the four key Josephson tunneling experiments on YBCO. The first one by Wollman *et al.*² on a YBCO-Pb corner junction is the simplest. We have shown that the phase of the supercurrent is independent of the choice of single-particle wave functions. In this experiment, tunneling occurs along the two perpendicular Cu-O bond directions in the CuO planes of YBCO (x and y axes) which are connected by a Pb wire. Pb is a BCS s -wave superconductor. A phase difference of π implies a d -wave gap, whereas no phase difference implies an s -wave gap. A d -wave result is obtained.

Let $T_{kp}^{(U,L)}(x)$ be the matrix element for tunneling a k electron in the U or L band to a p electron in Pb along the x axis. Choose the phase convention on the k states such that a 90° (C_4) rotation of the wave function for k is equal to the wave function for momentum C_4k . Then, we must have $T_{C_4k, C_4p}^{(U,L)}(y) = T_{kp}^{(U,L)}(x)$. From Eqs. (36) and (37), our phase convention gives

$$A_{U,L}(C_4k) = -A_{U,L}(k), \quad (56)$$

$$B_{U,L}(C_4k) = +B_{U,L}(k). \quad (57)$$

Using the gap equation and the expression (50) for $V_{k'k}$,

$$\Delta_k = \Delta(A_{Uk}B_{L-k} + B_{Uk}A_{L-k})^*. \quad (58)$$

Hence,

$$\Delta_{C_4k} = -\Delta_k, \quad (59)$$

leading to the result

$$J(C_4k \rightarrow C_4p) = -J(k \rightarrow p). \quad (60)$$

Therefore, our IBP model also gives an observed “ d -wave” gap.

For the tricrystal experiment of Tsuei *et al.*,³ we use the fact that for k near the Fermi surface touching point, ϕ_{Uk} has almost no d_{z^2} character and ϕ_{Lk} has almost no $d_{x^2-y^2}$ character or vice versa. For such a k vector, $B_{Uk} \approx 0$, $A_{Lk} \approx 0$ (or $A_{Uk} \approx 0$, $B_{Lk} \approx 0$) and we can take the phase convention A_{Uk} , B_{Lk} real with $A_{Uk} > 0$, $B_{Lk} > 0$ (or $B_{Uk} > 0$, $A_{Lk} > 0$). With this convention, Δ_k is real and $\Delta_k > 0$.

Suppose a $d_{x^2-y^2}$ orbital on one side of the grain boundary tunnels predominantly into a $d_{x^2-y^2}$ state on the other side of the boundary, and thus d_{z^2} on one side goes predomi-

nantly to d_{z^2} on the other side. Then, the matrix element for $d_{x^2-y^2} \rightarrow d_{x^2-y^2}$ is proportional to $\cos 2\theta \cos 2\phi$ where θ and ϕ are the orientations of the x and y axes in the CuO planes with respect to the grain boundary. Similarly, the $d_{z^2} \rightarrow d_{z^2}$ matrix element has no orientation dependence and is thus constant.

Suppose instead, that the dominant tunneling is $d_{x^2-y^2} \rightarrow d_{z^2}$ and $d_{z^2} \rightarrow d_{x^2-y^2}$. In this case, one matrix element is proportional to $\cos 2\theta$ and the other is proportional to $\cos 2\phi$ leading the pair tunneling product $\cos 2\theta \cos 2\phi$ as before.

Taking the product of the various factors in Eq. (53), we see that the phase controlling the current is the same as to be expected from a $d_{x^2-y^2}$ gap as is observed.

For the c -axis YBCO-Pb tunneling of Sun *et al.*,¹³ an analysis similar to the YBCO corner junction case shows that the interband pairs do not contribute to the current. In this case, the current due to BCS-like pairs must be considered. It is easy to see that if the dominant coupling of BCS-like pairs is to interband pairs as described above, then the BCS-like pairs are $d_{x^2-y^2}$ wave.

For the hexagonal YBCO tunneling of Chaudhari and Lin,¹⁴ the situation is different from the tricrystal YBCO in one very important manner. Here a hexagonal MgO layer is placed on the LaAlO₃ substrate and then YBCO is grown onto the sample. The hexagonal MgO causes YBCO to grow above it with its planar x , y axes rotated 45° from the angle of the YBCO grown directly over the LaAlO₃ substrate. Thus, we expect a misalignment of the CuO planes across the six junctions complicating the matrix elements that appear for interband pair tunneling. Unfortunately, we have been unable to find a convincing argument telling us whether interband or BCS-like pairs dominate the single-electron matrix elements in this case.

III. NORMAL-STATE NMR AND TRANSPORT

A. NMR

Armed with our parameters for the relevant bands and the criteria derived from IBP that the optimal doping is when the two Fermi surfaces touch, it is very easy to compute the normal-state NMR and transport properties using standard expressions for the NMR and the Bloch-Boltzmann equation for the transport. It is quite satisfying that not only can we understand qualitatively the numerous anomalous features of the NMR and transport as due to the character of the bands at this very special doping, but quantitatively the numbers are respectable.

The key normal-state NMR features⁵⁻¹¹ that a theory for the cuprates must explain are: (1) the difference in the relaxation rate curves with temperature T for the Cu and O nuclei in the plane, (2) the similar Knight shifts (KS) at the two sites, (3) the similarity of the O relaxation rate over T and the KS, (4) the lack of T dependence of the KS for optimally doped YBCO₇ and a monotonic increasing T dependence of the KS for optimally doped La-Sr-Cu-O and underdoped YBCO_{6.63}, (5) the strictly monotonic decreasing Cu relaxation rate over T for optimally doped YBCO₇ and the initially increasing and then decreasing Cu relaxation rate over T for underdoped YBCO_{6.63} and optimally doped La-Sr-Cu-O, and (6) the large anisotropy of the Cu relaxation rate for magnetic fields in the plane and along the z axis.

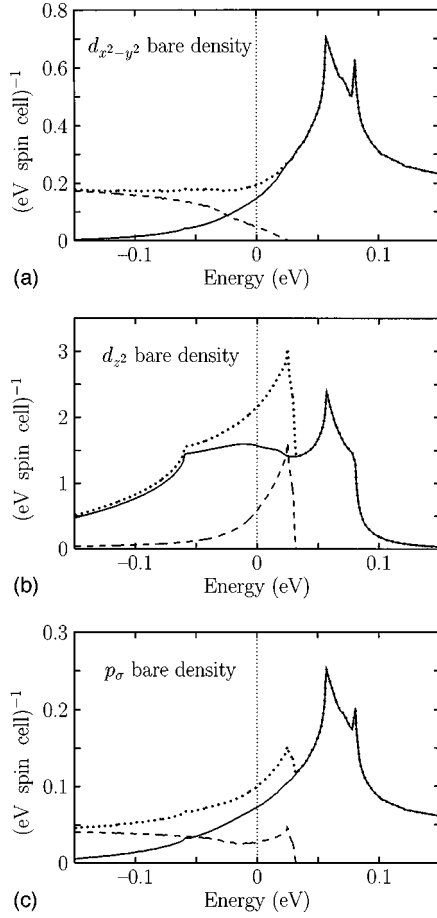


FIG. 6. Bare density of states for $d_{x^2-y^2}$, d_{z^2} , and p_{σ} orbitals for the U (solid line) and L (dashed line) bands and the total bare density of states (dotted line).

Figure 2 shows the two-band Fermi surfaces at optimal doping. The electronlike band centered at $k=(0,0)$ is the U (pper) band and the holelike surface centered around (π,π) is the L (ower) band. Both bands are occupied at $k=(0,0)$ and unoccupied at (π,π) .

Figure 3 shows the density of states for the two bands. The first thing to notice is that at the Fermi energy ϵ_F , the L band has the lower density of states. We expect that this band predominantly carries the current and being holelike will give a Hall coefficient with the correct sign. The large peak in the density of states of the U band at an energy a little larger (≈ 0.06 eV) than ϵ_F is due to the saddle-point singularity at $(\pi,0)$, $(0,\pi)$ for the U band. The width of the peak is due primarily to the overall strength of the z axis couplings. This width is very sensitive to the details of the structure. This sensitivity controls the T dependence of the KS. The other aspects of the density of states are robust.

Considering first the Cu spin relaxation, the two relevant orbitals are $d_{x^2-y^2}$ and d_{z^2} . Because there is no orbital relaxation between these orbitals regardless of the magnetic-field direction, the relevant relaxation is dipole-dipole. We will neglect here the core polarization relaxation which we expect will not change the qualitative conclusions. The relaxation rate for a z -axis magnetic field is given by

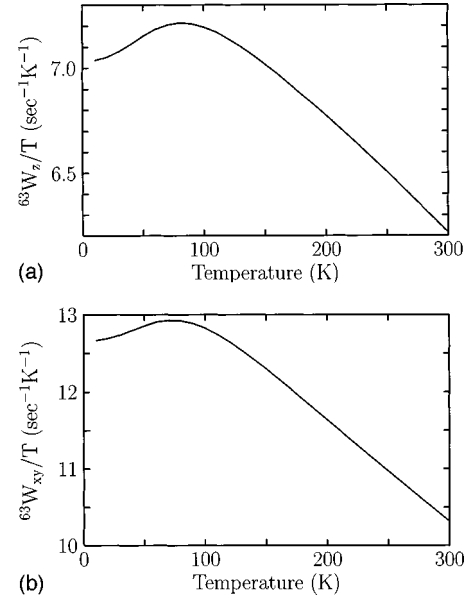


FIG. 7. Spin-relaxation rates over T of Cu for z axis and planar fields. In (b), the contribution due to d_{xy} is not included.

$${}^{63}W_z = 2 \left(\frac{2\pi}{\hbar} \right) (\gamma_e \gamma_h \hbar)^2 \int d\epsilon f(\epsilon) (1-f(\epsilon)) \times \left\langle \frac{1}{r^3} \right\rangle^2 [W_{\text{dip}}^z(\epsilon) + W_{\text{orb}}^z(\epsilon)], \quad (61)$$

$$W_{\text{dip}}^z(\epsilon) = \left(\frac{1}{7^2} \right) [6N_{d_{x^2-y^2}}(\epsilon)N_{d_{z^2}}(\epsilon) + N_{d_{x^2-y^2}}(\epsilon)N_{d_{x^2-y^2}}(\epsilon) + N_{d_{z^2}}(\epsilon)N_{d_{z^2}}(\epsilon)], \quad (62)$$

$$W_{\text{orb}}^z(\epsilon) = 0, \quad (63)$$

where $N(d_{x^2-y^2})(\epsilon)$ and $N(d_{z^2})(\epsilon)$ are the total bare density of states at energy ϵ and $f(\epsilon)$ is the Fermi-Dirac function.

The relaxation rate for a planar field ${}^{63}W_{xy}$ is identical to ${}^{63}W_z$ above with W_{dip}^z and W_{orb}^z replaced with

$$W_{\text{dip}}^{xy} = \left(\frac{1}{7^2} \right) \left(\frac{5}{2} \right) [N_{d_{x^2-y^2}}(\epsilon)N_{d_{x^2-y^2}}(\epsilon) + N_{d_{z^2}}(\epsilon)N_{d_{z^2}}(\epsilon)] + \left(\frac{3}{7^2} \right) N_{d_{x^2-y^2}}(\epsilon)N_{d_{z^2}}(\epsilon), \quad (64)$$

$$W_{\text{orb}}^{xy} = 0. \quad (65)$$

Figures 4(a) and 4(b) show the amount of orbital character of $d_{x^2-y^2}$ and d_{z^2} in the U and L bands. The total bare

density of states for d_{z^2} say, is the amount of orbital character of d_{z^2} in the U band times the density of states of the U band $N_U(\epsilon)$ plus a corresponding term for the L band. Figures 6(a)–6(c) are plots of the bare density of states for each orbital due to each band and the total bare density of states. In all calculations of the NMR and Hall effect, the temperature dependence of chemical potential has been taken into account. μ decreases about 5×10^{-3} eV from $T=0$ to $T=300$ K. Finally, plots of ${}^{63}W_z/T$ and ${}^{63}W_{xy}/T$ are shown in Figs. 7(a) and 7(b) where we have used the value²² $\langle 1/r^3 \rangle = 6$ a.u.. The curves show the characteristic peak at a T value greater than T_c and the order of magnitude of the rate is consistent with experiment.⁷ With the above figures and expressions for the relaxation rates we can qualitatively see why the correct behavior is obtained.

There are two different ways an electron may relax a Cu nucleus: one by intraband (U electron to U electron or L electron to L electron), or two, by the interband processes U to L and L to U . Due to the larger density of states of the U band, intraband L to L relaxation is small. This leaves the relaxation rate to be determined by the U to U intraband scattering and U to L (L to U) interband scattering. The U to U scattering leads to an increase of W/T due to the sharp increase in the U band density at the saddle-point singularity. On the other hand, the contribution from the interband term must decrease due to the closeness of the Fermi energy to the very top of the L band and therefore the vanishing of the density of states. The competition of these two terms gives the final result shown. Regarding the Cu KS, only the U to U contribution and L to L contribution can appear because the KS comes from diagonal elements of the electron-nuclear Hamiltonian. The U to U KS contribution dominates the L to L KS contribution due to the larger density of states of the U band as before leading to a monotonically increasing KS if the hyperfine couplings have the correct sign. The sign of the couplings will be discussed later on, but we can now see that the Cu KS and W/T will have different temperature dependences as observed.

It is pleasing to find that our calculated value for the relaxation rate has the correct order of magnitude (experimentally, ${}^{63}W_z/T \approx 20 \text{ s}^{-1} \text{ K}^{-1}$ at 100 K versus our value of $7.2 \text{ s}^{-1} \text{ K}^{-1}$). Our calculation has completely neglected the effects of the Cu $4s$ contact term and secondarily, the core polarization contribution. Also, our calculated percentage increase from 30 K to the peak is about 3% versus an experimental increase of ≈ 10 –20% and the percentage decrease from the peak value to the 300 K value is 15% versus the observed ≈ 50 %. In spite of these differences, the qualitative behavior is correct and this is the most important aspect given the level of calculation used in deriving the Hubbard model parameters.

As we can see from Figs. 7(a) and 7(b), the relaxation anisotropy of ≈ 3.4 is not accounted for with the present model. What is missing here is a small amount of d_{xy} orbital character in our bands. d_{xy} is the next most unstable Cu orbital by ligand field theory after $d_{x^2-y^2}$ and d_{z^2} . Including some d_{xy} character affects W_{xy} dramatically because now orbital relaxation is permitted $W_{\text{orb}}^{xy} \neq 0$, whereas W_{orb}^z remains zero. Including d_{xy} makes

$$W_{\text{orb}}^{xy}(\epsilon) = 4N_{d_{x^2-y^2}}(\epsilon)N_{d_{xy}}(\epsilon), \quad (66)$$

$$W_{\text{orb}}^z = 0. \quad (67)$$

There are also additional terms due to d_{xy} in the dipole-dipole terms (62), (64) but these are small and cannot account for the anisotropy. We neglect them here.

The coefficient of 4 in front of W_{orb}^{xy} is about 30 times larger than the first coefficient in Eq. (62) and more than two orders of magnitude greater than the other coefficients in W_{dip}^z . Thus, d_{xy} character on the order of a few percent will lead to a contribution to ${}^{63}W_{xy}$ as large as the dipole term leading easily to an anisotropy factor commensurate with experiment.

For the planar O sites, the relevant orbital is p_σ . The O $2s$ will be considered later. The lack of a second major O orbital near the Fermi surface and also the fact that at (π, π) there is no mixing of antibonding (most unstable) p_σ (symmetry B_{1g}) with d_{z^2} (A_{1g}) are the differences between O and Cu that lead to the different spin-relaxation rate temperature dependences. Figure 4(c) shows the amount of p_σ character on an O site at various energies. Figure 6(c) shows the p_σ bare density of states due to the U and L bands and the total bare density of states.

We can see that the contribution to the bare density of states due to the L band $N_{L,p_\sigma}(\epsilon)$ is small compared to the U band term $N_{U,p_\sigma}(\epsilon)$ leading to a small contribution to the relaxation rate due to the L band. This is due to the L band k states near the Fermi energy being close to (π, π) . At (π, π) , d_{z^2} couples to the neighboring σ orbitals which must be in a bonding configuration. This bonding set of σ orbitals is stabilized by the $t_{\sigma\sigma}$ term. Thus, to create the most unstable d_{z^2} configuration at (π, π) , we cannot have a large amount of p_σ character leading to the small value for $N_{L,p_\sigma}(\epsilon)$ near the Fermi energy.

There are three distinct directions for the magnetic field at the O site with different relaxation rates. These are the z -axis normal to the CuO planes, the σ axis along the Cu-O bond direction, and the perpendicular axis \perp normal to z and σ . With only the p_σ to consider, the relaxation along z and \perp are equal, ${}^{17}W_z = {}^{17}W_\perp \neq {}^{17}W_\sigma$.

The expressions for ${}^{17}W_z$, ${}^{17}W_\sigma$ are of the same form as for Cu Eq. (61) with the crude approximation $\langle 1/r^3 \rangle \approx 3$ a.u. determined by *ab initio* calculations and γ_n the gyromagnetic ratio of the ${}^{17}\text{O}$ nucleus. With only a p_σ contributing, there is no orbital relaxation in any direction of the magnetic field

$${}^{17}W_{\text{orb}}^z = {}^{17}W_{\text{orb}}^\sigma = {}^{17}W_{\text{orb}}^\perp = 0. \quad (68)$$

The dipole-dipole relaxation term is

$$W_{\text{dip}}^\sigma = \left(\frac{1}{5^2} \right) N_{p_\sigma}(\epsilon) N_{p_\sigma}(\epsilon), \quad (69)$$

$$W_{\text{dip}}^z = W_{\text{dip}}^\perp = \left(\frac{5}{2} \right) W_{\text{dip}}^\sigma. \quad (70)$$

A plot of the ${}^{17}W_\sigma$ relaxation is shown in Fig. 8. The others are simply 2.5 times larger. This relaxation is monotonic increasing due to the bare density of p_σ due to the L band being small.

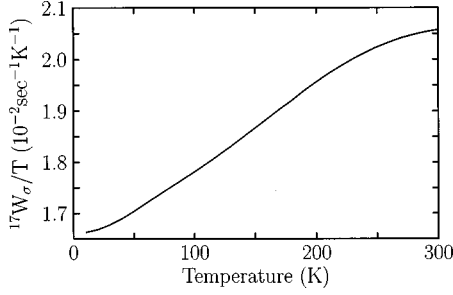


FIG. 8. Relaxation rate over T for O with field along Cu-O bond direction.

There remains one orbital that can make a large contribution to the relaxation due to its large hyperfine coupling to the nucleus that we have not yet considered. That is the O $2s$ orbital. A very small amount of $2s$ can have a large effect on ^{17}W without making any change in our calculated band structure. At (π, π) , the L band has no $d_{x^2-y^2}$ character and by symmetry no $2s$ character either. Thus, similar to $N_{Lp_\sigma}(\epsilon)$, there is almost no contribution to the O $2s$ bare density $N_{2s}(\epsilon)$ due to the L band leading to the same monotonic increasing behavior as in Fig. 8. O $2s$ will make a large change to the absolute value of the relaxation rate. Without estimating the size of the $2s$ contribution, we cannot compare our answer in Fig. 8 to experimental data on La-Sr-Cu-O. Without O $2s$, the values in Fig. 8 are about an order of magnitude too small.⁷

The KS on the O sites is due to the O $2s$ Fermi contact interaction, the p_σ orbital dipole coupling, and core polarization. In Fig. 9, we simply plot the KS,

$$K_\sigma = -2K_z = -2K_\perp = \left(\frac{8}{5}\right) \left\langle \frac{1}{r^3} \right\rangle \mu_B^2 \int \left(-\frac{\partial f}{\partial \epsilon} \right) N_{p_\sigma}(\epsilon) d\epsilon, \quad (71)$$

due to the p_σ dipole-dipole term. Since the $2s$ and core polarization shifts are isotropic, our curve may be compared to the axial KS, $K_{\text{ax}} = 2(K_\sigma - K_\perp)/3$. The monotonic increase in the shift is due to the sharp increase in the U band density of states above ϵ_F due to the saddle-point singularity at $(\pi, 0)$, $(0, \pi)$.

The KS involves only one factor of $N_{p_\sigma}(\epsilon)$, while the relaxation contains $N_{p_\sigma}(\epsilon)^2$. Thus, there is no way $^{17}W/T \propto K_\sigma$ is strictly possible, although from the figures, the agreement is not far off.

For the Cu KS, we need to introduce the effects of the Cu $4s$ orbital and the two p_z orbitals above and below the Cu on the apical oxygens. Experimentally, the Cu KS for a z -axis field is T independent, while for planar fields the shift is monotonic increasing with increasing T . As we discussed, the dominant contribution to the shift will come from the bare density of states for the orbitals from the U bands. If we can somehow show that the hyperfine couplings are positive for planar fields and zero for the z -axis field, then we should expect a curve similar to Fig. 9 for Cu KS.

The Cu KS along the z -axis and planar directions is the sum of

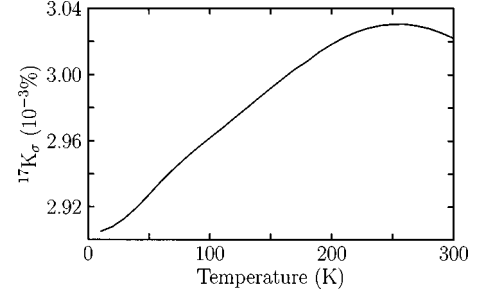


FIG. 9. O σ direction Knight shift due to p_σ .

$${}^{63}K_\alpha = K_\alpha^{\text{dip}}(d_{x^2-y^2}) + K_\alpha^{\text{dip}}(d_{z^2}) + K_\alpha^{\text{contact}}(4s) + K_\alpha^{\text{cp}} + K_\alpha^{\text{dip}}(d_{z^2}, 4s), \quad (72)$$

where α is the field direction z or planar, $K^{\text{dip}}(d_{x^2-y^2})$, $K^{\text{dip}}(d_{z^2})$ are the dipole shifts due to the $d_{x^2-y^2}$ and d_{z^2} orbitals, $K^{\text{contact}}(4s)$ is the Fermi contact shift, K^{cp} is the core polarization shift, and $K^{\text{dip}}(d_{z^2}, 4s)$ is the dipole contribution due to the interference of d_{z^2} and $4s$. The expressions for the first four terms are

$$\begin{aligned} K_z^{\text{dip}}(d_{x^2-y^2}) &= -2K_{xy}^{\text{dip}}(d_{x^2-y^2}) \\ &= -\frac{8}{7} \left\langle \frac{1}{r^3} \right\rangle \mu_B^2 \int \left(-\frac{\partial f}{\partial \epsilon} \right) N_{d_{x^2-y^2}}(\epsilon) d\epsilon, \end{aligned} \quad (73)$$

$$\begin{aligned} K_z^{\text{dip}}(d_{z^2}) &= -2K_{xy}^{\text{dip}}(d_{z^2}) \\ &= +\frac{8}{7} \left\langle \frac{1}{r^3} \right\rangle \mu_B^2 \int \left(-\frac{\partial f}{\partial \epsilon} \right) N_{d_{z^2}}(\epsilon) d\epsilon, \end{aligned} \quad (74)$$

$$\begin{aligned} K_z^{\text{contact}}(4s) &= K_{xy}^{\text{contact}}(4s) \\ &= \frac{16\pi}{3} |\psi_{4s}(0)|^2 \mu_B^2 \int \left(-\frac{\partial f}{\partial \epsilon} \right) N_{4s}(\epsilon) d\epsilon, \end{aligned} \quad (75)$$

$$\begin{aligned} K_z^{\text{cp}} &= K_{xy}^{\text{cp}} = -(2\alpha) \left\langle \frac{1}{r^3} \right\rangle \mu_B^2 \int \left(-\frac{\partial f}{\partial \epsilon} \right) \\ &\quad \times [N_{d_{x^2-y^2}}(\epsilon) + N_{d_{z^2}}(\epsilon)] d\epsilon. \end{aligned} \quad (76)$$

We take the value $\alpha = 0.33$ (dimensionless) from Abragam and Bleaney.²² $\psi_{4s}(0)$ is the value of the $4s$ orbital at the nucleus.

The d_{z^2} , $4s$ interference term is evaluated by taking the mean value of a band wave function at the Fermi surface with the dipole Hamiltonian. Let

$$\phi_k = A_k d_{x^2-y^2k} + B_k d_{z^2k} + C_k \psi_{4sk} + \dots, \quad (77)$$

where $d_{x^2-y^2k}$, d_{z^2k} are defined in Eqs. (34), (35) and ψ_{4sk} is defined similarly. Then,

$$\langle \phi_k | H_{\text{dip}} | \phi_k \rangle = (-2\mu_B)(\gamma_n \hbar) [I_x S_x + I_y S_y - 2I_z S_z] \cdot \left\{ \left(-\frac{2}{7} \left\langle \frac{1}{r^3} \right\rangle \right) |A_k|^2 + \left(+\frac{2}{7} \left\langle \frac{1}{r^3} \right\rangle \right) |B_k|^2 + \left(\frac{1}{\sqrt{5}} \left\langle \frac{1}{r^3} \right\rangle \right)_{z^2,s} \right. \\ \left. \times (B_k^* C_k + B_k C_k^*) \right\} + \text{term involving } (A_k^* C_k + A_k C_k^*), \quad (78)$$

$$\left\langle \frac{1}{r^3} \right\rangle_{z^2,s} = \int_0^{+\infty} r^2 dr R_{d_{z^2}}(r) \left(\frac{1}{r^3} \right) R_{4s}(r), \quad (79)$$

where I is the nuclear spin and $R_{d_{z^2}}(r)$, $R_{4s}(r)$ are the radial parts of the d_{z^2} and $4s$ orbitals, respectively, with normalizations

$$\int_0^{+\infty} r^2 dr R_{d_{z^2}}(r)^2 = \int_0^{+\infty} r^2 dr R_{4s}(r)^2 = 1. \quad (80)$$

Averaging over the Fermi surface, the interference term $A_k C_k^* + A_k^* C_k$ due to $d_{x^2-y^2}$ and $4s$ becomes zero due to the different symmetries of $d_{x^2-y^2}$ and $4s$ (B_{1g} and A_{1g}). The first two terms in Eq. (78) lead to $K^{\text{dip}}(d_{x^2-y^2}) + K^{\text{dip}}(d_{z^2})$ and the third term gives

$$K_z^{\text{dip}}(d_{z^2}, 4s) = \left(\frac{8}{\sqrt{5}} \right) \left\langle \frac{1}{r^3} \right\rangle_{z^2,s} \mu_B^2 \int \left(-\frac{\partial f}{\partial \epsilon} \right) \langle B_k^* C_k \rangle N(\epsilon) d\epsilon, \quad (81)$$

$$K_{xy}^{\text{dip}}(d_{z^2}, 4s) = -\frac{1}{2} K_z^{\text{dip}}(d_{z^2}, 4s), \quad (82)$$

where $\langle B_k^* C_k \rangle$ is the mean value of $B_k^* C_k$ over the Fermi surface and $N(\epsilon)$ is the total density of states of the band. Depending on the sign of $\langle B_k^* C_k \rangle$, the shift due to the interference term can be positive enhancing the field due to d_{z^2} , or negative decreasing the net magnetic field of d_{z^2} . The bare d_{z^2} and $4s$ density of states from this band are $\langle |B_k|^2 \rangle N(\epsilon)$ and $\langle |C_k|^2 \rangle N(\epsilon)$. Since only one power of C_k appears in Eq. (81), $\langle B_k^* C_k \rangle$ can be large although $\langle |C_k|^2 \rangle$ may be small.

The bare $d_{x^2-y^2}$ density of states is smaller than the d_{z^2} density of states at the Fermi energy leading to a net positive shift from $K(d_{x^2-y^2}) + K(d_{z^2})$ along the z direction and a net negative shift along the plane. $K^{\text{contact}}(4s)$ is isotropic and always positive.

At all k vectors on the Fermi surface, the d_{z^2} and p_z 's on the apical O form an antibonding combination leading to a larger amount of $4s$ character than one expects from a $d_{x^2-y^2}$ band. Thus, if the d_{z^2} , $4s$ interference term leads to a negative $\langle B_k^* C_k \rangle$ that is sufficiently large, the net effect of $K(d_{x^2-y^2}) + K(d_{z^2}) + K(d_{z^2}, 4s)$ leads to a dipolar field which is negative in the z direction and positive along the plane. We shall assume that due to the charge donation of the apical O p_z to the Cu $4s$, this is the case. With this assumption, we can see how the net shift on the Cu due to a z -axis field can add to zero while simultaneously leading to positive shifts for planar fields. In Eq. (72), the contribution to K_x

from the contact and core polarization terms should be a net isotropic positive value. Without the interference shift (81), there is no way the z -axis shift can add to zero. Figure 10 shows the T dependence of the z -axis shift of $K(d_{x^2-y^2})$ and $-K(d_{z^2})$. These curves have approximately the same T dependence as the O shift and $^{17}W/T$.

The above considerations also show why for fully doped YBCO₇, the T dependence of the shifts and $^{17}W/T$ are almost constant. If there is more dispersion in the z direction of the d_{z^2} orbital, then the saddle-point peak in the U band density of states will be broadened. If the plateau is sufficiently broad to extend all the way to the Fermi energy or the $(\pi, 0)$ and $(0, \pi)$ saddle-point singularity is sufficiently far away from the Fermi energy, then the shifts and O relaxation will become T independent. For optimally doped YBCO₇, there are no vacancies in the chains and one can expect more 3D dispersion from the d_{z^2} orbital.

B. Hall effect and resistivity

Since the density of states for the L band is smaller than for the U band in the vicinity of the Fermi energy at the crossing point, we take the L band as the primary carrier of current. The Hall coefficient R_H is the ratio of the transverse conductivity σ_{xy} and the conductivity σ squared. Using standard Boltzmann theory²³

$$\sigma_{xy} = \left(\frac{m_e^2 \Omega_0}{\hbar} \right) \left(\frac{1}{\Omega} \right) \sum_k \left(-\frac{\partial f}{\partial \epsilon_k} \right) v_{k_y} \left[v_{k_y} \frac{\partial}{\partial k_x} - v_{k_x} \frac{\partial}{\partial k_y} \right] v_{k_x}, \quad (83)$$

$$\sigma = m_e \Omega_0 \left(\frac{1}{\Omega} \right) \sum_k \left(-\frac{\partial f}{\partial \epsilon_k} \right) v_{k_x}^2, \quad (84)$$

$$R_H = \left(\frac{\Omega_0}{qc} \right) \frac{\sigma_{xy}}{\sigma^2}, \quad (85)$$

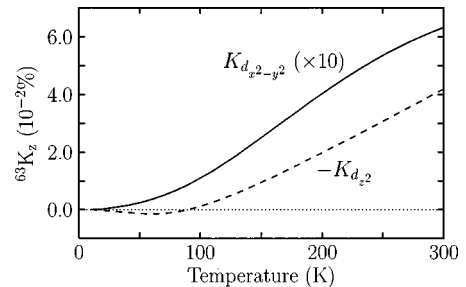


FIG. 10. The z -axis Cu Knight shifts. $K_{d_{x^2-y^2}}$ has been multiplied by 10 in this graph. The $T=0$ values have been subtracted.

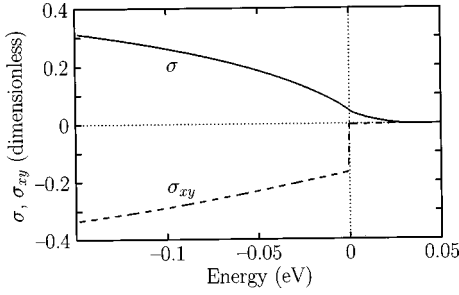


FIG. 11. Plots of the L band $\sigma_{xy}(\epsilon)$ and $\sigma(\epsilon)$.

where m_e is the electron mass, Ω_0 is the primitive unit-cell volume $\Omega_0 = 96 \text{ \AA}^3$, Ω is the total volume, $q = -|e| < 0$ is the electron charge, and c is the velocity of light. $v_k = \nabla_k \epsilon_k / \hbar$ is the velocity. We have multiplied σ_{xy} and σ by the appropriate factors of m_e and Ω_0 to make the expressions in Eqs. (82) and (83) dimensionless and have neglected the scattering rate $1/\tau$ in these expressions because for R_H , τ does not appear. We may also define $\sigma_{xy}(\epsilon)$ and $\sigma(\epsilon)$ by replacing the Fermi-Dirac function $-\partial f / \partial \epsilon_k$ by the delta function $\delta(\epsilon_k - \epsilon)$ in Eqs. (82) and (83). Then

$$\sigma_{xy} = \int \sigma_{xy}(\epsilon) \left(-\frac{\partial f}{\partial \epsilon_k} \right) d\epsilon, \quad (86)$$

$$\sigma = \int \sigma(\epsilon) \left(-\frac{\partial f}{\partial \epsilon_k} \right) d\epsilon. \quad (87)$$

Figure 11 is a plot of $\sigma_{xy}(\epsilon)$ and $\sigma(\epsilon)$ and Fig. 12 shows the temperature dependence of the Hall coefficient at optimal doping. The absolute magnitude of R_H is about ten times larger than observed values for La-Sr-Cu-O, but the calculated percentage change of R_H from 100–300 K is $\approx 40\%$ in good agreement with experiment¹² ($\approx 50\%$).

These curves were calculated taking the small z -axis dispersion parameters $T_{(0,0)}$, $T_{(\pi,0)}$, and $T_{(\pi,\pi)}$ in Eqs. (31)–(33) to be zero. This was done to simplify the computation. $\sigma_{xy}(\epsilon)$ changes very rapidly for energies higher than the Fermi energy at the band touching point, whereas the change in $\sigma(\epsilon)$ is not as dramatic.

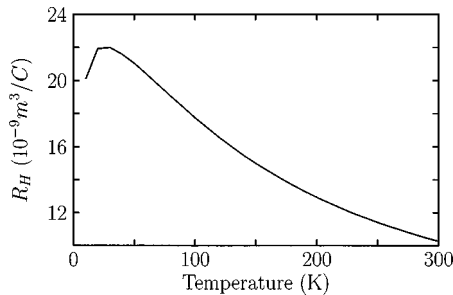


FIG. 12. Temperature dependence of the L band Hall coefficient.

The abrupt change in $\sigma_{xy}(\epsilon)$ is due to the two-band crossing point. Near the Fermi energy of the crossing point, the repulsion of the two bands for nondiagonal k vectors strongly affects the shape of the two Fermi surface leading to a large curvature for the L band. At energies slightly higher than the Fermi energy, the L band surface is not affected by the presence of the U band and the Fermi surface becomes “small” leading to the reduced curvature. The overall T dependence of R_H is due to the combined T dependences of both σ and σ_{xy} rather than solely due to σ_{xy} as one would expect from a first glance at Fig. 11. We can see that the presence of the two-band crossing point and the association of optimal superconductivity with this point is the root cause of the strong anomalous temperature dependence of the Hall coefficient.

There are several possible explanations for our calculated value for R_H being more than ten times too large. The most obvious one is the neglect of next-nearest-neighbor hopping terms in our Hubbard model. The second cause is due to our 2D approximation to the band structure. A more detailed description than ours of the z -axis dispersion is required. The third reason is the neglect of the contribution from the electronlike surface of the U band. Finally, more refined *ab initio* calculations than the ones performed in the following paper on the CuO_6 complex embedded in the point-charge field of La-Sr-Cu-O will change the parameters used in our Hubbard model.

The resistivity due to scattering with phonons should be linear at the optimal doping for two reasons: (1) the Fermi surface for the L band is “small,” and (2) at optimal doping the electron current can strongly relax by scattering to a U electron state. At optimal doping, the U band Fermi surface touches the L band surface leading to nearby states in k space with very different currents. The T dependence of σ complicates this scenario because σ is proportional to the effective number of charge carriers in the band. It is unclear how the T dependence of the relaxation rate $1/\tau$ could cancel this dependence. If a full-blown 3D model was used instead of our 2D model with the third dimension included as a perturbation, we believe that the temperature dependence of σ would become small while σ_{xy} would remain very T dependent.

IV. CONCLUSIONS

We have presented a model for superconductivity of the cuprates based on the idea that Cooper pairs are formed from electrons between two distinct bands. This leads naturally to associating optimal doping with a Fermi surface touching point of the two bands. We have postulated the character of the two bands to arise from $d_{x^2-y^2}$, d_{z^2} , $O p_\sigma$, and apical $O p_z$ orbitals. A Hubbard model for these bands is setup and we calculate some normal-state consequences of the model. With our model, many of the anomalous features of the normal-state NMR, Hall effect, and resistivity are explained qualitatively and to varying degrees quantitatively. The primary reason for the anomalous normal-state properties is due to the optimal doping being at the Fermi-surface touching point.

We show that interband pairing alters the standard interpretation of Josephson tunneling. With interband pairs, the

detailed nature of the single-particle tunneling matrix elements plays a prominent role. We show that with this piece of physics, three of the four Josephson tunneling experiments are explained by our model with a phonon-mediated attractive coupling.

The parameters in the Hubbard model used in this paper

are derived in the following paper by Perry and Tahir-Kheli from calculations on a CuO_6 cluster for $\text{La}_{2-x}\text{Sr}_x\text{CuO}_4$. We conclude there that contrary to band-structure calculations where only one band with Cu $d_{x^2-y^2}$ and O p_σ character is found, two bands exist at the Fermi energy with the character described above.

-
- ¹J. Tahir-Kheli, in *Proceedings of the 10th Anniversary HTS Workshop on Physics, Materials and Applications*, edited by B. Batlogg, C. W. Chu, W. K. Chu, D. U. Gubser, and K. A. Müller (World Scientific, Singapore, 1996), p. 491.
- ²D. A. Wollman, D. J. van Harlingen, W. C. Lee, D. M. Ginsberg, and A. J. Leggett, *Phys. Rev. Lett.* **71**, 2134 (1993).
- ³C. C. Tsuei, J. R. Kirtley, C. C. Chi, Lock See Yu-Jahnes, A. Gupta, T. Shaw, J. Z. Sun, and M. B. Ketchen, *Phys. Rev. Lett.* **73**, 593 (1994).
- ⁴J. K. Perry and J. Tahir-Kheli, following paper, *Phys. Rev. B* **58**, 12 323 (1998).
- ⁵M. Takigawa, P. C. Hammel, R. H. Heffner, Z. Fisk, K. C. Ott, and J. D. Thompson, *Phys. Rev. Lett.* **63**, 1865 (1989).
- ⁶M. Takigawa, P. C. Hammel, R. H. Heffner, Z. Fisk, J. L. Smith, and R. B. Schwarz, *Phys. Rev. B* **39**, 300 (1989).
- ⁷R. E. Walstedt, B. S. Shastry, and S-W. Cheong, *Phys. Rev. Lett.* **72**, 3610 (1994).
- ⁸T. Imai, K. Yoshimura, T. Uemura, H. Yasuoka, and K. Kosuge, *J. Phys. Soc. Jpn.* **59**, 3846 (1990).
- ⁹M. Takigawa, A. P. Reyes, P. C. Hammel, J. D. Thompson, R. H. Heffner, Z. Fisk, and K. C. Ott, *Phys. Rev. B* **43**, 247 (1991).
- ¹⁰R. E. Walstedt, W. W. Warren, Jr., R. F. Bell, G. F. Brennert, G. P. Espinosa, R. J. Cava, L. F. Schneemeyer, and J. V. Waszczak, *Phys. Rev. B* **38**, 9299 (1988).
- ¹¹M. Horvatić, C. Berthier, Y. Berthier, P. Ségransan, P. Butaud, W. G. Clark, J. A. Gillet, and J. Y. Henry, *Phys. Rev. B* **48**, 13 848 (1993).
- ¹²H. Y. Hwang, B. Batlogg, H. Takagi, H. L. Kao, J. Kwo, R. J. Cava, J. J. Krajewski, and W. F. Peck, Jr., *Phys. Rev. Lett.* **72**, 2636 (1994).
- ¹³A. G. Sun, D. A. Gajewski, M. B. Maple, and R. C. Dynes, *Phys. Rev. Lett.* **72**, 2267 (1994).
- ¹⁴P. Chaudhari and Shawn-Yu Lin, *Phys. Rev. Lett.* **72**, 1084 (1994).
- ¹⁵H. Takagi, R. J. Cava, M. Marezio, B. Batlogg, J. J. Krajewski, W. F. Peck, Jr., P. Boudet, and D. E. Cox, *Phys. Rev. Lett.* **68**, 3777 (1992).
- ¹⁶R. J. Cava, B. Batlogg, C. H. Chen, E. A. Rietman, S. M. Zahurak, and D. Werder, *Nature (London)* **329**, 423 (1987).
- ¹⁷H. Takagi, B. Batlogg, H. L. Kao, J. Kwo, R. J. Cava, J. J. Krajewski, and W. F. Peck, Jr., *Phys. Rev. Lett.* **69**, 2975 (1992).
- ¹⁸P. G. deGennes, *Superconductivity of Metals and Alloys* (Addison-Wesley, Reading, MA, 1966).
- ¹⁹Z.-X. Shen, D. S. Dessau, B. O. Wells, D. M. King, W. E. Spicer, A. J. Arko, D. Marshall, L. W. Lombardo, A. Kapitulnik, P. Dickinson, S. Doniach, J. DiCarlo, A. G. Loeser, and C. H. Park, *Phys. Rev. Lett.* **70**, 1553 (1993).
- ²⁰M. R. Norman, H. Ding, M. Randeria, J. C. Campuzano, T. Yokoya, T. Takeuchi, T. Takahashi, T. Mochiku, K. Kadowaki, P. Guptasarma, and D. G. Hinks, *Nature (London)* **392**, 157 (1998).
- ²¹J. K. Perry and J. Tahir-Kheli (unpublished).
- ²²A. Abragam and B. Bleaney, *Electron Paramagnetic Resonance of Transition Ions* (Dover, New York, 1986), p. 458.
- ²³J. M. Ziman, *Electrons and Phonons* (Oxford University Press, Oxford, 1960).